J|A|C|S
ARTICLES
Published on Web 07/26/2002

XMCD Characterization of the Ferromagnetic State of $Yb_{14}MnSb_{11}$

Aaron P. Holm,[†] Susan M. Kauzlarich,*[,†] Simon A. Morton,[‡] G. Dan Waddill,[‡] Warren E. Pickett,[§] and James G. Tobin[⊥]

Contribution from the Departments of Chemistry and Physics, University of California, One Shields Avenue, Davis, California 95616, Department of Physics, University of Missouri—Rolla, Rolla, Missouri 65401-0249, and Lawrence Livermore National Laboratory, Livermore, California 94550

Received April 22, 2002

Abstract: X-ray magnetic circular dichroism (XMCD) measurements on $Yb_{14}MnSb_{11}$ provide experimental evidence of a moment of 5 μ_B on Mn, with partial cancellation by an opposing moment on the Sb_4 cage surrounding each Mn ion. The compound is isostructural to $Ca_{14}AlSb_{11}$, with Mn occupying the Al site in the $AlSb_4^{9-}$ discrete tetrahedral, anionic unit. Bulk magnetization measurements indicate a saturation moment of 3.90 ± 0.02 μ_B/formula unit consistent with four unpaired spins and implying a Mn^{3+}, high-spin d^4 state. XMCD measurements reveal that there is strong dichroism in the Mn L_{23} edge, the Sb M_{45} edge shows a weak dichroism indicating antialignment to the Mn, and the Yb N_{45} edge shows no dichroism. Comparisons of the Mn spectra with theoretical models for Mn^{2+} show excellent agreement. The bulk magnetization can be understood as Mn with a moment of 5 μ_B and a 2+ configuration, with cancellation of one spin by an antialigned moment from the Sb 5p band of the Sb_4 cage surrounding the Mn.

I. Introduction

The family of transition metal compounds with the $Ca_{14}AlSb_{11}$ structure type[1] has shown a wide variety of unique electronic and magnetic properties.[2,3] In particular, the series $A_{14}MnPn_{11}$ show properties ranging from paramagnetic insulators to ferromagnetic metals, depending on the identity of A (alkaline earth or rare earth atom) and Pn (pnictogen atom). This class of compounds consists of an isolated magnetic cluster that can magnetically couple over large interionic distances (~1 nm). The magnetic exchange interaction has been attributed to a Ruderman—Kittel—Kasuya—Yosida (RKKY) interaction between localized moments via conduction electrons.[3] This structure type ($A_{14}MPn_{11}$) can be prepared with most 2+ cations, such as A = Ca, Sr, Ba, Eu, and Yb, with M = Mn, Al, Ga, In, Nb, and Zn, and with Pn = P, As, Sb, and Bi.[1—26] One formula unit is composed of 14 A^{2+} cations, 1 MPn_4^{9-} tetrahedron, 1 Pn_3^{7-} unit, and 4 Pn^{3-} isolated anions. The structure has been interpreted according to the Zintl concept, which invokes charge balance between (usually) closed shell structural units such as complexes or extended covalent structures and ions. In this

* Address correspondence to this author. E-mail: smkauzlarich@ucdavis.edu.
[†] Department of Chemistry, University of California—Davis.
[§] Department of Physics, University of California—Davis.
[‡] Department of Physics, University of Missouri—Rolla.
[⊥] Lawrence Livermore National Laboratory.

(1) Cordier, G.; Schäfer, H.; Stelter, M. *Z. Anorg. Allg. Chem.* **1984**, *519*, 183.
(2) Kauzlarich, S. M. In *Chemistry, Structure, and Bonding of Zintl Phases and Ions*; Kauzlarich, S. M., Ed.; VCH Publishers: New York, 1996; pp 245—274.
(3) Kauzlarich, S. M.; Payne, A. C.; Webb, D. J. In *Magnetism: Molecules to Materials III*; Miler, J. S., Drillon, M., Eds.; Wiley-VCH: Weinham, 2002; pp 37—62.
(4) Kauzlarich, S. M., Ed. *Chemistry, Structure, and Bonding of Zintl Phases and Ions*; VCH Publishers: New York, 1996.
(5) Brock, S. L.; Weston, L. J.; Olmstead, M. M.; Kauzlarich, S. M. *J. Solid State Chem.* **1993**, *107*, 513—523.
(6) Chan, J. Y.; Kauzlarich, S. M.; Klavins, P.; Shelton, R. N.; Webb, D. J. *Chem. Mater.* **1997**, *9*, 3132—3135.
(7) Chan, J. Y.; Olmstead, M. M.; Kauzlarich, S. M.; Webb, D. J. *Chem. Mater.* **1997**, *10*, 3583—3588.
(8) Chan, J. Y.; Wang, M. E.; Rehr, A.; Kauzlarich, S. M.; Webb, D. J. *Chem. Mater.* **1997**, *9*, 2131—2138.
(9) Chan, J. Y.; Kauzlarich, S. M.; Klavins, P.; Shelton, R. N.; Webb, D. J. *Phys. Rev. B* **1998**, *57*, 8103—8106.
(10) Chan, J. Y.; Kauzlarich, S. M.; Klavins, P.; Liu, J.-Z.; Shelton, R. N.; Webb, D. J. *Phys. Rev. B* **2000**, *61*, 459—463.
(11) Del Castillo, J.; Webb, D. J.; Kauzlarich, S. M.; Kuromoto, T. Y. *Phys. Rev. B* **1993**, *47*, 4849—4852.
(12) Fisher, I. R.; Wiener, T. A.; Bud'ko, S. L.; Canfield, P. C.; Chan, J. Y.; Kauzlarich, S. M. *Phys. Rev. B* **1999**, *59*, 13829—13834.
(13) Gallup, R. F.; Fong, C. Y.; Kauzlarich, S. M. *Inorg. Chem.* **1992**, *31*, 115—118.
(14) Kauzlarich, S. M.; Kuromoto, T. Y.; Olmstead, M. M. *J. Am. Chem. Soc.* **1989**, *111*, 8041—8042.
(15) Kauzlarich, S. M.; Kuromoto, T. Y. *Croat. Chem. Acta* **1991**, *64*, 343—352.
(16) Kauzlarich, S. M.; Thomas, M. M.; Odink, D. A.; Olmstead, M. M. *J. Am. Chem. Soc.* **1991**, *113*, 7205—7208.
(17) Kuromoto, T. Y.; Kauzlarich, S. M.; Webb, D. J. *Mol. Cryst. Liq. Cryst.* **1989**, *181*, 349—357.
(18) Kuromoto, T. Y.; Kauzlarich, S. M.; Webb, D. J. *Chem. Mater.* **1992**, *4*, 435—440.
(19) Payne, A. C.; Olmstead, M. M.; Kauzlarich, S. M.; Webb, D. J. *Chem. Mater.* **2001**, *13*, 1398—1406.
(20) Rehr, A.; Kauzlarich, S. M. *J. Alloys Compd.***1994**, *207*, 424—426.
(21) Rehr, A.; Kuromoto, T. Y.; Kauzlarich, S. M.; Del Castillo, J.; Webb, D. J. *Chem. Mater.* **1994**, *6*, 93—99.
(22) Siemens, D. P.; Del Castillo, J.; Potter, W.; Webb, D. J.; Kuromoto, T. Y.; Kauzlarich, S. M. *Solid State Commun.* **1992**, *84*, 1029—1031.
(23) Webb, D. J.; Kuromoto, T. Y.; Kauzlarich, S. M. *J. Magn. Magn. Mater.* **1991**, *98*, 71—75.
(24) Webb, D. J.; Kuromoto, T. Y.; Kauzlarich, S. M. *J. Appl. Phys.* **1991**, *69*, 4825.
(25) Webb, D. J.; Cohen, R.; Klavins, P.; Shelton, R. N.; Chan, J. Y.; Kauzlarich, S. M. *J. Appl. Phys.* **1998**, *83*, 7192—7194.
(26) Young, D. M.; Torardi, C. C.; Olmstead, M. M.; Kauzlarich, S. M. *Chem. Mater.* **1995**, *7*, 93—101.

10.1021/ja020564y CCC: $22.00

simple model, the Mn is 3+, similar to group 13 metals that also crystallize in this structure type. Both structure and magnetism measurements have been used to support this assignment.[3]

Recently, colossal magnetoresistance (CMR) has been discovered in some of the compounds of this structure type.[6,9,10,12,19,27] The proposal that the CMR effect could be closely associated with, or resulting from, a half-metallic nature[28,29] makes the CMR compounds possible half-metallic ferromagnets. The recent commercial development of spin-polarized electronic transport devices for use in magnetic information storage has initiated great interest in new materials possessing unique magnetic and electronic properties for direct applications in magnetoelectronic devices.[30] There is great interest in developing conducting materials that possess 100% spin-polarization at the Fermi level, a class of materials that de Groot et al. first termed half-metallic ferromagnets (HMFMs).[31] A large number of ternary intermetallic compounds including the spinels, such as Fe_3O_4,[32] the various Heusler phases, such as Mn_2VAl,[33] and the half-Heusler alloys, most notably NiMnSb and PtMnSb,[31,34−36] have been indicated by calculations to be half-metallic ferromagnets. Compounds with the perovskite structure, $La_{0.7}Ca_{0.3}MnO_3$[28] and $La_{0.7}Sr_{0.3}MnO_3$,[37] and the double perovskite structure, Sr_2FeMoO_6,[38,39] are also strong candidates for half-metallicity. In addition, a few much simpler binary compounds, such as CrO_2 and some compounds of the Zinc blende structure, are also suggested as half-metals.[29,40−43]

To gain more insight into the coupling of the carriers with the magnetic order, a first-principles density-functional study of the electronic properties of two compounds, $Ca_{14}MnBi_{11}$, which orders ferromagnetically, and $Ba_{14}MnBi_{11}$, which orders antiferromagnetically, has been performed.[44] This study indicates that these phases are nearly half-metallic, and that Mn is present in this structure as Mn^{2+}. It also predicts the presence of a polarized hole localized on the $MnPn_4$ tetrahedron lying parallel to the Mn moment, and resulting in a net $MnPn_4$ moment that is considerably reduced from the ionic Mn^{2+} value.

In this paper, we take advantage of the elemental specificity allowed in X-ray magnetic circular dichroism (XMCD) to probe the specific nature of the magnetic moment on the elements in the Zintl compound, $Yb_{14}MnSb_{11}$. The XMCD effect results from a difference in the absorption of right and left circularly polarized X-rays by a magnetically polarized sample. It originates in the interchange of spin−orbit interaction in the initial state and the angular momentum conservation in the absorption process that reflects the local spin and orbital polarization of the final states.[45] $Yb_{14}MnSb_{11}$ was the compound of choice because we are able to grow large single crystals of this phase. Single crystals are important because it has been shown that the magnetization parallel and perpendicular to the *c*-axis is highly anisotropic.[12] Our XMCD results clearly indicate a large dichroism signal within the Mn L_{23} edge due to a magnetic moment present on the Mn, a small antialigned moment on Sb as revealed in the Sb M_{45} edge, and no moment on Yb as observed in the Yb N_{45} edge. When coupled with the bulk magnetization value of $\sim 4\ \mu_B$/formula unit, these results demonstrate that ferromagnetic alignment of the unpaired Mn spins is achieved, and there is a small moment on Sb that is antialigned with the Mn moment. The XMCD results are reconciled with the bulk magnetic measurements.

II. Experimental Section

A. Sample Preparation. Single-crystal samples of $Yb_{14}MnSb_{11}$ were grown by a high-temperature molten metal flux synthesis as described elsewhere.[12,46] Several different batches of crystals have been studied by both magnetic measurements and XMCD. There are no differences between sample batches in the measured XMCD spectra and magnetic properties measurements.

B. Magnetic Measurements. Full magnetic and transport measurements have been published.[7,12] The crystals used in this experiment were characterized by single-crystal magnetic susceptibility. Direct current magnetization data were obtained with a Quantum Design MPMS Superconducting Quantum Interference Device (SQUID) magnetometer with a 7 T superconducting magnet. Data were collected and analyzed with the Magnetic Property Measurement System (MPMS) software provided. The crystal was placed in a gel capsule and suspended in a straw. The orientation was determined by a series of magnetization vs field measurements and aligned according to the easy magnetization axis (*c*-axis). Magnetization vs temperature data (Figure 2) were obtained, and a Curie temperature (T_C) of $\sim$53 K was measured, consistent with previously published results.[7,12] The crystals were measured before and after all the XMCD measurements to verify the integrity of the samples.

C. XMCD Data Collection and Analysis. The XMCD measurements of Mn L_{23}, Sb M_{45}, and Yb N_{45} edges were performed using the elliptically polarized undulator (EPU) of Beamline 4.0 at the Advanced Light Source with 90% circularly polarized light.[47−49] The spectra were measured using the total photoelectron yield method by detecting the sample current as a function of photon energy through the absorption edge while alternating helicity at each point. Crystals have been taken from different batches, and all the results are reproducible. The base chamber pressure was maintained at better than 1×10^{-9} Torr throughout the experiments. Single-crystal samples of $Yb_{14}MnSb_{11}$ were mounted on a copper sample stage fit with permanent magnets of Ni-coated NdFeB alloy rated at a magnetic field of 4000 G. Taking advantage of the anisotropic magnetization, samples were oriented with the magnetically easy axis (*c*-axis) along the Poynting vector. The sample stage was cooled to and maintained at a temperature of less than 20 K throughout the experiments. Clean surfaces were obtained

(27) Kim, H.; Chan, J. Y.; Olmstead, M. M.; Klavins, P.; Webb, D. J.; Kauzlarich, S. M. *Chem. Mater.* **2002**, *14*, 206−216.
(28) Pickett, W. E.; Singh, D. J. *Phys. Rev. B* **1996**, *53*, 1146−1160.
(29) Pickett, W. E.; Moodera, J. S. *Phys. Today* **2001**, May, 39−44.
(30) Prinz, G. A. *Science* **1998**, *282*, 1660−1663.
(31) de Groot, R. A.; Mueller, F. M.; van Engen, P. G.; Buschow, K. H. J. *Phys. Rev. Lett.* **1983**, *50*, 2024−2027.
(32) Irkhin, V. Y.; Katsnel'son, M. I. *Usp. Fiz. Nauk* **1994**, *164*, 705−724.
(33) Weht, R.; Pickett, W. E. *Phys. Rev. B* **1999**, *60*, 13006−13010.
(34) de Groot, R. A.; Buschow, K. H. J. *J. Magn. Magn. Mater.* **1986**, *54−57*, 1377−1380.
(35) Kulatov, E.; Mazin, I. I. *J. Phys.: Condensed Matter* **1990**, *2*, 343−350.
(36) Moodera, J. S.; Mootoo, D. M. *J. Appl. Phys.* **1994**, *76*, 6101−6103.
(37) Park, J. H.; Vescovo, E.; Kim, H. J.; Kwon, C.; Ramesh, R.; Venkatesan, T. *Nature* **1998**, *392*, 794−796.
(38) Kise, T.; Ogasawara, T.; Ashida, M.; Tomioka, Y.; Tokura, Y.; Kuwata-Gonokami, M. *Phys. Rev. B* **2000**, *85*, 1986−1989.
(39) Kobayashi, K.-I.; Kimura, T.; Sawada, H.; Terakura, K.; Tokura, Y. *Nature* **1998**, *395*, 677−680.
(40) Ji, Y.; Strijkers, G. J.; Yang, F. Y.; Chien, C. L.; Byers, J. M.; Anguelouch, A.; Xiao, G.; Gupta, A. *Phys. Rev. Lett.* **2001**, *86*, 5585−5588.
(41) Lewis, S. P.; Allen, P. B.; Sasaki, T. *Phys. Rev. B* **1997**, *55*, 10253−10260.
(42) Brener, N. E.; Tyler, J. M.; Callaway, J.; Bagayoko, D.; Zhao, G. L. *Phys. Rev. B* **2000**, *61*, 16582−16588.
(43) Schwarz, K. *J. Phys. F* **1986**, *16*, L211−215.
(44) Sánchez-Portal, D.; Martin, R. M.; Kauzlarich, S. M.; Pickett, W. E. *Phys. Rev. B* **2002**, *65*, 144414−144415.
(45) Kapusta, C.; Fischer, P.; Schütz, G. *J. Alloys Compd.* **1999**, *286*, 37−46.
(46) Canfield, P. C.; Fisk, Z. *Philos. Mag. B* **1992**, *65*, 1117−1123.
(47) Tobin, J. G.; Waddill, G. D.; Pappas, D. P. *Phys. Rev. Lett.* **1992**, *68*, 3642−3645.
(48) Tobin, J. G.; Waddill, G. D.; Jankowski, A. F.; Sterne, P. A.; Pappas, D. P. *Phys. Rev. B* **1995**, *52*, 6530−6541.
(49) Young, A. T.; Martynov, V.; Padmore, H. A. *J. Electron Spectrosc. Relat. Phenom.* **1999**, *101−103*, 885−889.

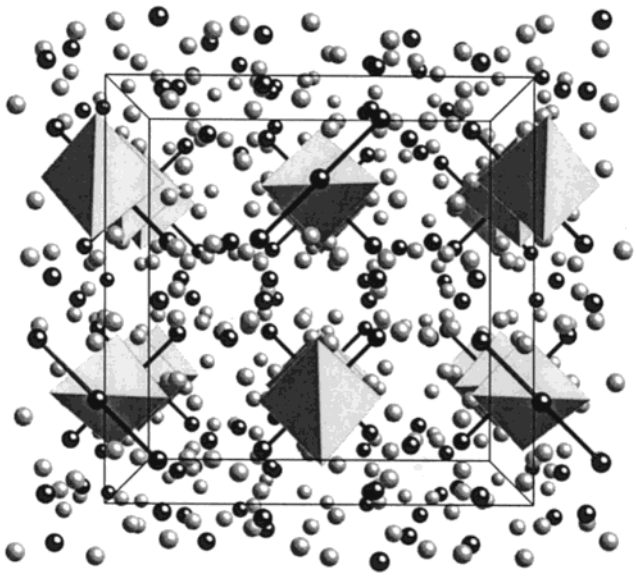

Figure 1. Perspective view down the *c*-axis of the crystal structure of $Yb_{14}MnSb_{11}$. The $MnSb_4$ tetrahedra (shown as polyhedra) alternate with the Sb_3 linear units shown in black. The isolated Sb atoms are also shown in black, and the Yb atoms are shown in gray.

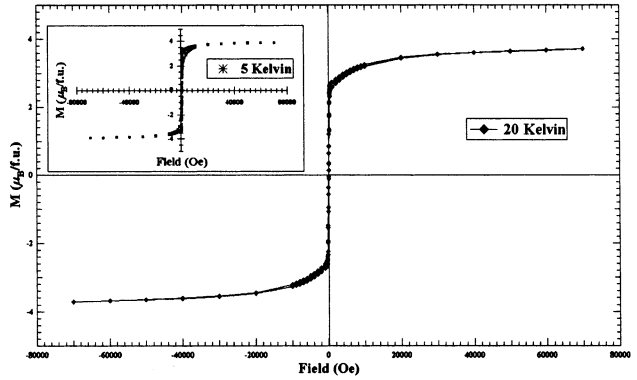

Figure 2. Magnetic hysteresis loops measured at $T = 20$ and 5 K (inset) of single crystals of $Yb_{14}MnSb_{11}$ aligned with the crystallographic *c*-axis parallel to the applied magnetic fields.

by cleaving the samples in situ with a two-blade cleaving tool and comparing the resulting left- and right-polarized Mn L_{23} XAS spectra to the same for the uncut spectra.

Special consideration is given in analyzing the Mn XMCD spectrum with a comparison to previously reported calculations of the magnetically ordered Mn^{2+} and Mn^{3+} XMCD spectra in spherical crystal field symmetry ($\Delta = 0$).[50] The spectra calculated with spherical symmetry were considered adequate for comparison due to the high-spin tetrahedral symmetry of the Mn d orbitals in the anionic unit. The calculated difference spectra were digitized and convoluted using commercially available software packages in the energy range 637−655 eV with an energy-dependent Gaussian function based on the full width at half-maximum value of the raw experimental spectra. The convolution of the calculated spectra was performed in order to approximate experimental lifetime broadening effects.

III. Discussion

A. Structure. The $Yb_{14}MnSb_{11}$ structure is shown in Figure 1. The structure has been analyzed in detail many times, but for this paper it is important to note the isolation of the tetrahedra (there is no extended bonding network) and the distortion of the tetrahedra. The tetrahedra are surrounded by a cage of Yb^{2+} cations and stack in an alternating pattern, with Sb linear anions along the *c*-axis giving an effective Mn···Mn distance of 1 nm between each tetrahedron. Each $MnSb_4^{9-}$ tetrahedron is compressed perpendicular to the *ab* plane, distorting the anion from the ideal tetrahedral angle of 109.5° to the complementary angles of 117.5 and 105.6°. The deformation in the $MnSb_4^{9-}$ tetrahedral anion has always been attributed to a Jahn−Teller distortion due to an assignment of the Mn as a d^4 ion.[3]

B. Magnetism. The dc magnetization data are presented in Figure 2 for a single crystal of $Yb_{14}MnSb_{11}$ at 20 and 5 K (inset) aligned along the easy magnetization axis (*c*-axis). The temperature of 20 K was chosen to be consistent with the XMCD measurements. The observed saturation moment of 3.90 ± 0.02 μ_B/formula unit is consistent with the expected value of 4 μ_B/Mn assigned to four unpaired electrons on an Mn^{3+} ion. This interpretation is the simplest that provides an overall accounting of charge for the $MnSb_4^{9-}$ anion and the additional structural distortion. $Yb_{14}MnSb_{11}$ has been characterized electronically as well. In short, the temperature dependence of the electrical resistivity is metallic, with a significant loss of spin-disorder scattering at the ferromagnetic transition temperature, and with the application of magnetic fields, the resistivity drops, broadening the transition associated with the loss of spin-disorder scattering.[12]

C. X-ray Magnetic Circular Dichroism. XMCD measurements were carried out in order to gain a better understanding of the ferromagnetic and magnetoresistive behavior observed in this compound. The advantage in using this technique is the ability to specifically probe each element of the system, and to identify the magnetic contribution of each constituent to the total magnetic moment.[47,48,51] Measurements of the Mn L_{23}, Sb M_{45}, and Yb N_{45} absorption edges for both +0.9 and −0.9 helicity are given in Figure 3.

Figure 3a displays the absorption spectra for the Mn L_{23} edge. A significant dichroism is apparent and is consistent with the magnetic ordering arising from the Mn component of the system. The $2p_{3/2}$ core excitation region of both the I+ and I− spectra display a sharp peak structure, with additional shoulder structure in the I− spectrum just to the lower energy side of the main peak and farther along on the high energy side. The $2p_{1/2}$ component presents a clear doublet structure with an interchange in the relative intensity of the two components of the doublet between the I+ and the I− spectra. In addition, due to a greater intensity of the higher energy component of the doublet, the I− spectrum's $2p_{1/2}$ component appears to have broadened slightly in relation to the I+ spectrum.

The absorption spectrum for the Sb M_{45} region is shown in Figure 3b. It shows a great deal of structure reflecting the complexity of the system due to the multiple crystallographic sites of Sb (four total). The spin−orbit split components for the $3d \rightarrow 5p$ transition ($3d_{5/2}$ and $3d_{3/2}$) are present at a separation of approximately 10 eV at positions consistent with what is expected for Sb (528.2 and 537.5 eV, respectively). In addition, a broad multiplet is present, with an onset at approximately 530 eV and a sharp peak at about 534 eV that is due to the O1s absorption edge. There is also another broad, low-intensity peak centered at approximately 543 eV that does not appear to reveal any type of shoulder or multiplet structure.

(50) van der Laan, G.; Thole, B. T. *Phys. Rev. B* **1991**, *43*, 13401−13411.

(51) Goering, E.; Will, J.; Geissler, J.; Justen, M.; Weigand, F.; Schuetz, G. *J. Alloys Compd.* **2001**, *328*, 14−19.

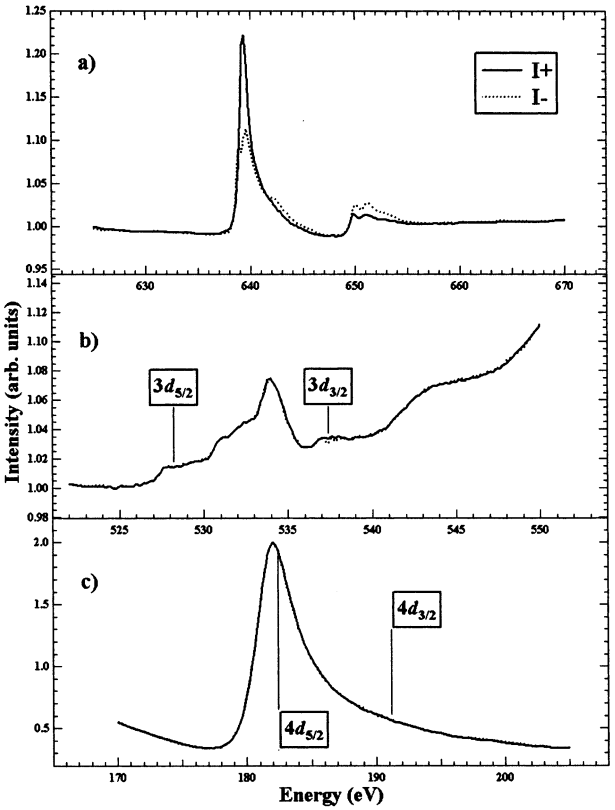

Figure 3. Raw absorption spectra for (a) Mn L_{23}, (b) Sb M_{45}, and (c) Yb N_{45}. The solid curve (dashed curve) indicates the absorption intensity with the light polarization positive (negative), as denoted by I+ (I−).

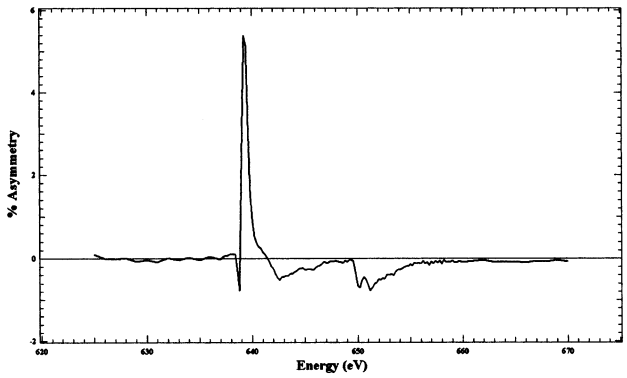

Figure 4. Mn L_{23} XMCD spectrum in terms of % asymmetry = [(I+) − (I−)]/[(I+) + (I−)] × 100.

The Yb N_{45} absorption spectra in Figure 3c demonstrate no dichroism, consistent with a nonmagnetic assignment due to a closed shell Yb^{2+} configuration. The observation of a single peak for the Yb 4d doublet is consistent with previous observations of Yb^{2+} with a small amount of surface oxidation.[52] This result is not surprising due to the multiple sites of Yb tending to wash out the second peak of the doublet, and also due to previous observations of a rapid formation of surface oxidation associated with the Yb.[7,52]

The XMCD spectrum for Mn, shown in Figure 4 in terms of percent asymmetry, demonstrates a sharp, low-intensity negative signal at the L_3 edge onset followed by a prominent positive and another small, but much broader, negative component within the $2p_{3/2}$ core excitation region. The $2p_{1/2}$ region of the spectrum displays a small negative signal with a sharp doublet peak structure. The general peak structures and peak positions are in agreement with previously reported XAS and XMCD spectra of some related Mn-based alloys.[51,53]

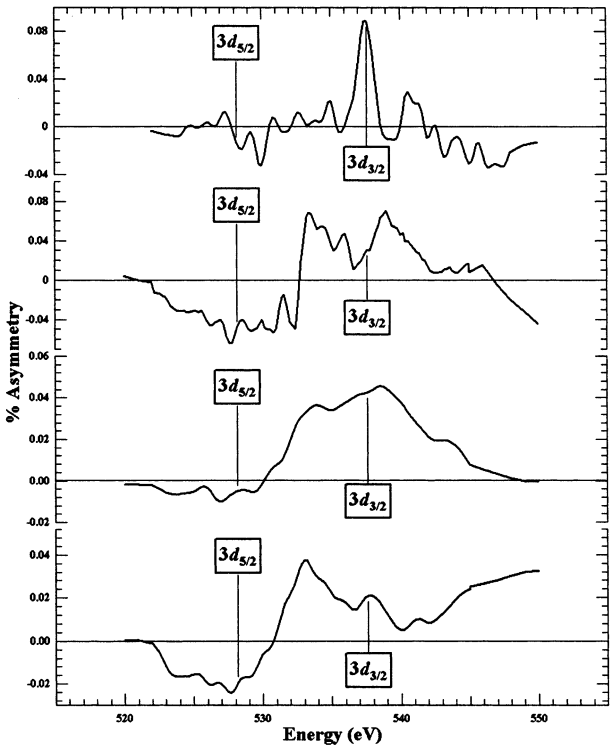

Figure 5. Sb M_{45} XMCD spectra in terms of % asymmetry for four separate crystal samples.

A series of XMCD spectra of the Sb M_{45} region from different samples are shown in Figure 5. These spectra demonstrate that the general behavior of the Sb dichroism, although small, is reproducible from sample to sample. Small but clearly negative and positive signals respectively are present for the $3d_{5/2}$ and $3d_{3/2}$ absorption components. The $3d_{3/2}$ component is quite sharp in intensity at the expected energy, but the $3d_{5/2}$ XMCD signal is less than half the intensity of the related component and is shifted to slightly higher energy from the expected position of this component. The observed dichroism signal is antialigned to the Mn dichroism signal. This result is unusual and exactly opposite to what is observed in the case of Mn and Sb for the half-Heusler alloy, NiMnSb.[53] The XMCD spectra of NiMnSb show dichroism for both Mn and Sb. However, the dichroism signals from both the Mn and Sb dichroism show the same positive and negative alignment: the Mn $2p_{3/2}$ and Sb $3d_{5/2}$ signals are positive, and the Mn $2p_{1/2}$ and Sb $3d_{3/2}$ signals are negative. The alignment of signals has been attributed to an induced moment on Sb that is antialigned to the Mn moment. This result is due to the fact that the d → p transition probability for Sb should be polarized opposite to the Mn p → d transition if the moments were aligned in the same direction.[53] Mn in NiMnSb is in an octahedral crystal field, whereas Mn in $Yb_{14}MnSb_{11}$ is in a tetrahedral field. Therefore, the experimental results for $Yb_{14}MnSb_{11}$ should show an opposite spin-polariza-

(52) Formichev, V. A.; Gribovskii, S. A.; Zimkina, T. M. *Sov. Phys., Solid State* **1974**, *15*, 1880−1881.

(53) Kimura, A.; Suga, S.; Shishidou, T.; Imada, S.; Muro, T.; Park, S. Y.; Miyahara, T.; Kaneko, T.; Kanomata, T. *Phys. Rev. B* **1997**, *56*, 6021−6030.

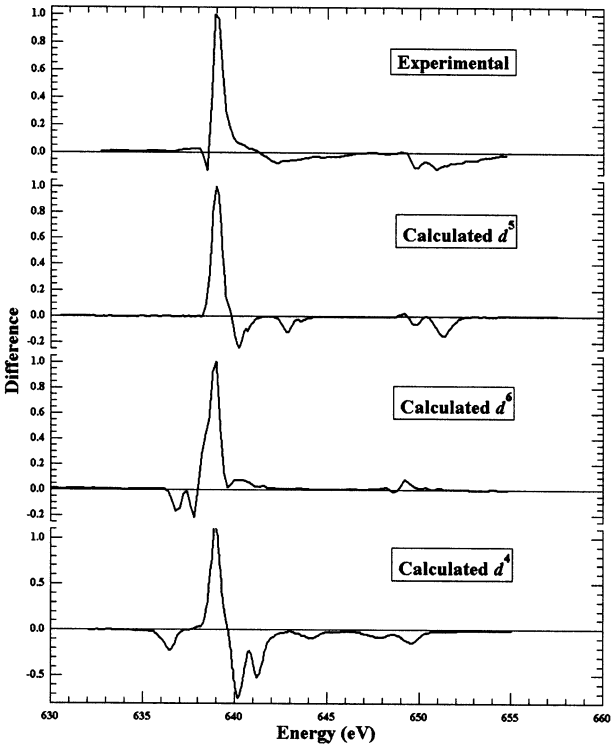

Figure 6. Mn L_{23} XMCD spectra showing a comparison (from top to bottom) of the experimental, calculated d^5, calculated d^6, and calculated d^4 ions in spherical symmetry ($\Delta = 0$). The calculated spectra are taken directly from ref 49 without any further treatment.

tion relationship if the spins are antialigned. This is consistent with our experimental results. The XMCD spectra for $Yb_{14}MnSb_{11}$ indicate that there is a moment on Sb that is antialigned to the Mn.

Figure 6 shows a comparison of the experimental dichroic difference with atomic calculations of the magnetically ordered Mn^{2+} and Mn^{3+} ions calculated in octahedral symmetry ($\Delta = 0$).[50] This type of comparison was chosen over a direct calculation of the magnetic moment using a sum rules approach due to the inability for sum rules to accurately account for the multielectronic effects possibly present on the Mn, and also the inability for sum rules to account for the crystal field effects that influence this system.[54,55] The atomic calculations of van der Laan and Thole provide these necessary requirements with the ability to make comparisons between various crystal fields and oxidation states, and they are also able to model the prominent multiplet structures in these spectra. There are no published calculations of the absorption spectra for the magnetically ordered Mn ions in tetrahedral symmetry, but a direct correlation to tetrahedral symmetry can be made using the simple relation $d^n(\text{tetr}) \equiv d^{10-n}(\text{oct})$.[56] Therefore, the calculated spectra for Mn d^5 (for Mn^{2+}) and Fe d^6 (for Mn^{3+}) from ref 49 were used, in addition to the Cr d^4 spectrum for further comparison. It is clear from Figures 6 and 7 that the best agreement between calculation and experiment is the Mn d^5 (Mn^{2+}) spectrum. There is extremely poor agreement between the calculated spectrum for the Mn^{3+} ion and the experimental

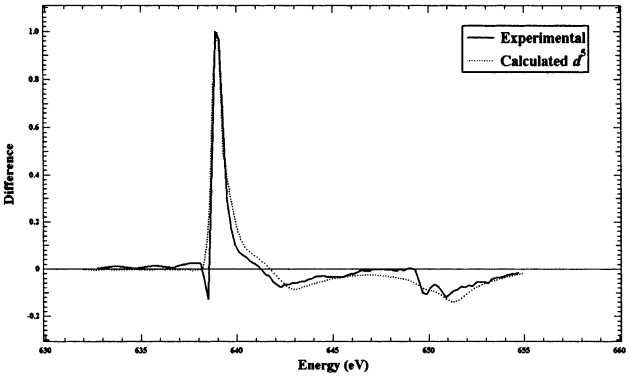

Figure 7. Direct comparison of the experimental Mn L_{23} XMCD spectrum (solid line) and the convoluted calculated d^5 spectrum.

data. However, the valence assignment for Mn as 2+ appears to be inconsistent with the bulk magnetization data, and appears to contradict the valence assignment and charge balance previously given.[2,3,6−12,14,17−25] A recent theoretical study of the bonding, moment formation, and magnetic interactions of the related $Ca_{14}MnBi_{11}$ and $Ba_{14}MnBi_{11}$ systems suggests a new model to account for the discrepancy between electron counting and the experimental data.[44] Using an efficient, local orbital-based method within the local spin density approximation, it was found that Mn is indeed high-spin d^5, but that the bonding bands are one electron per formula unit short of being filled. Even though this arrangement would leave the Mn 3d states fully occupied, the $\sim 4\ \mu_B$/formula unit experimental magnetic moment would be maintained due to a hole (unoccupied cluster orbital) in the Pn_4 tetrahedron aligning parallel to the Mn moment, and the unpaired electron associated with the hole aligning antiparallel to the Mn moment.

IV. Summary

The XMCD spectrum for the Sb M_{45} region shows a small dichroism effect that indicates antialignment of a small moment on Sb with the moment on Mn, supporting the prediction of a hole on the Pn valence p states of the tetrahedron lying parallel to the moment on Mn. The element-specific measurements furnished by X-ray magnetic circular dichroism and the explanation of the spectral behavior offered by theory are in excellent agreement with the bulk magnetization data showing $4\ \mu_B$. We are continuing to address new questions that have been raised by our recent results and are extending our experiments to explore further the wide range of magnetic behavior displayed by the $A_{14}MnPn_{11}$ family of materials. This will enable us to significantly improve our understanding of these complex magnetic systems.

Acknowledgment. We thank R. N. Shelton for use of the magnetometer and P. Klavins for technical assistance. We also thank the staff of the Advanced Light Source and Beamline 4.0 for their assistance. This research is funded by the National Science Foundation DMR-9803074, 0120990, by the Materials Research Institute through LLNL, and by Campus Laboratory Collaborations Program of the University of California, and was performed under the auspices of the U.S. Department of Energy by Lawrence Livermore National Laboratory under Contract No. W-7405-Eng-48.

JA020564Y

(54) Carra, P.; Thole, B. T.; Altarelli, M.; Wang, X. *Phys. Rev. Lett.* **1993**, *70*, 694−697.
(55) Thole, B. T.; Carra, P.; Sette, F.; van der Laan, G. *Phys. Rev. Lett.* **1992**, *68*, 1943−1946.
(56) Cotton, F. A. *Chemical Applications of Group Theory*, 3rd ed.; John Wiley and Sons: New York, 1990.